Energy Storage Materials 32 (2020) 418–424

Contents lists available at ScienceDirect

Energy Storage Materials

journal homepage: www.elsevier.com/locate/ensm

# Laser writing of the restacked titanium carbide MXene for high performance supercapacitors

Jun Tang [a,b], Wendi Yi [a], Xiongwei Zhong [a], Chuanfang (John) Zhang [c], Xu Xiao [d], Feng Pan [b,**], Baomin Xu [a,*]

[a] Department of Materials Science and Engineering, Southern University of Science and Technology, Shenzhen, Guangdong Province, 518055, PR China
[b] School of Advanced Materials, Peking University Shenzhen Graduate School, Peking University, Shenzhen, Guangdong Province, 518055, PR China
[c] Laboratory for Functional Polymers, Swiss Federal Laboratories for Materials Science and Technology, Empa, ETH Domain, Überlandstrasse 129, CH-8600, Dübendorf, Switzerland
[d] Department of Materials Science and Engineering and A. J. Drexel Nanomaterials Institute, Drexel University, Philadelphia, PA, 19104, USA

ARTICLE INFO

*Keywords:*
Titanium carbide MXene
Restacking
Laser
High-rate
Supercapacitors

ABSTRACT

Titanium carbide MXene ($Ti_3C_2T_x$, where $T_x$ refers to -Cl, –F, –OH and = O) shows ultrahigh electronic conductivity but restricted rate performance for supercapacitors due to prolonged ion transport caused by the restacking of 2D materials. In this work, an ultrafast laser writing technique is used for alleviating the restacking issue by opening up the restacked layers and creating pores through instantaneous photothermal gasification of interlayer water and partial surface groups. The rate performance of $Ti_3C_2T_x$ film is effectively improved after laser writing. By tuning the line density of laser scanning path, the electrochemical performance can be well controlled and an optimized high capacitance of 322 F $g^{-1}$ at 10 mV $s^{-1}$ is obtained at relative high rate performance, showing a high capacitance retention of 48% as the scan rate increased by 200-fold. As a result, the symmetric microsupercapacitor with laser written $Ti_3C_2T_x$ electrodes exhibits a high areal capacitance of 15.03 mF $cm^{-2}$ at 10 mV $s^{-1}$ with ultrahigh capacitance retention of 33% at 2000 mV $s^{-1}$. Moreover, the laser writing process takes only ~1 s for an 1 cm × 1 cm square film, showing superior advantages over other methods and potentials in scale-up production.

## 1. Introduction

The rapid growing demands for high performance power-supplies require energy storage devices to deliver high energy density at relatively high charge/discharge rates. Pseudocapacitors are capable to store more charge via fast redox reaction compared to that of electrical double layer capacitors (EDLCs) which relies on the electrostatic ion adsorption [1–5]. Typical electrode materials for pseudocapacitors such as $RuO_2$ [6,7], $MnO_2$ [8,9], VN [10,11] and conductive polymers [12,13] have shown high capacitances (for example, up to 1585 F $g^{-1}$ was achieved by $RuO_2$ [14]). Most of these materials exhibit high ion accessibility with nanostructured architecture and opened channels [15–17]. But the low electronic conductivity of these pseudocapacitor materials always result in undesirable performances.

As a rapidly expanding class of two-dimensional (2D) materials, MXenes (transition metal carbides, nitrides and carbonitrides) have shown a great potential in electrochemical energy storage applications [18–27]. As the mostly studied MXene, titanium carbide $Ti_3C_2T_x$ ($T_x$ refers to the surface groups such as -Cl, –F, –OH and –O) exhibits excellent pseudocapacitive performance due to the high electronic conductivity (up to 15000 S $cm^{-1}$) and high proton-induced pseudocapacitance in acid-based aqueous electrolytes [28–30]. High packing density (up to 4 g $cm^{-3}$, close to the density of metals), along with high pseudocapacitance endow $Ti_3C_2T_x$ with ultrahigh volumetric capacitance (up to 1500 F $cm^{-3}$) [31]. However, the rate performance is still relatively unsatisfactory for high conductive $Ti_3C_2T_x$-based electrodes because of the restacking issue of 2D materials. The severe restacking phenomenon of $Ti_3C_2T_x$ nanosheets hinders the out-of-plane electron transport and largely prolongs the electrolyte ion transport distance inside the film electrode [32].

Numerous efforts have been made to address the restacking issue of $Ti_3C_2T_x$ nanosheets. Central to these endeavors are opening the

* Corresponding author.
** Corresponding author.
*E-mail addresses:* panfeng@pkusz.edu.cn (F. Pan), xubm@sustech.edu.cn (B. Xu).

https://doi.org/10.1016/j.ensm.2020.07.028
Received 1 May 2020; Received in revised form 10 July 2020; Accepted 19 July 2020
Available online 28 July 2020

interlayer channels of the dense stacked films (such as intercalation of nanomaterials, constructing 3D architecture, pillared structure design) and shortening the ion transport pathway (such as reducing the flake size, etching holes) [33–38], etc. An ideal method should be effective, facile, easily scalable, environmental friendly, low-cost and compatible with manufacturing process for $Ti_3C_2T_x$-based devices. However, few of the reported methods satisfies all the requirements. Intercalation of nanomaterials is an widely used facile method but degrades the inherent high performance of $Ti_3C_2T_x$. For example, a 5 wt% intercalation of graphene results into a decrease of ~15% in volumetric capacitance due to the lower packing density of graphene [35]. Some methods are time consuming such as frozen-drying for opened 3D channels, which usually take hours to days. Template sacrifice method is an effective method for building 3D structured $Ti_3C_2T_x$ film, as reported by Lukatskaya et al. for example, but the synthesized process is complicated with lots of steps [31]. Overall, most of the methods need a mix of $Ti_3C_2T_x$ suspension with other chemicals or nanomaterials, which will inevitably affect the stability of the colloid since the dispersion of $Ti_3C_2T_x$ nanosheets is based on the electrostatic repulsion. In other words, it is quite a challenge to develop a facile and effective way without affecting the dispersity of $Ti_3C_2T_x$ colloid (up to 100 mg $mL^{-1}$ in water) unless the treatment is introduced post film formation.

Herein, an ultrafast laser writing treatment is reported for alleviating the restacking issue of $Ti_3C_2T_x$ film. The ion channels between dense stacked $Ti_3C_2T_x$ nanosheets can be effectively opened up by laser as a result of photothermal gasification of adsorbed $H_2O$ molecules and some oxygen-containing terminations. Moreover, plenty of holes are generated after laser writing due to the oxidation induced by the photothermal effect. The modified structure after laser greatly facilitates the ion transport inside the $Ti_3C_2T_x$ film and significantly improves the rate performance. Compared with other methods for the restacking issues, contactless and chemical-free laser writing is an ultrafast and facile post-treatment which takes only seconds for improving the rate performance of $Ti_3C_2T_x$ for supercapacitors. Since the laser writing is a local high temperature treatment, it is even compatible with flexible devices with plastic substrates, which shows great potential in scale-up fabrication of high performance power supply for wearable electronics.

## 2. Results and discussions

Single-layer $Ti_3C_2T_x$ nanoflakes are generally synthesized by selectively etching the Al atoms from its MAX precursor ($Ti_3AlC_2$) followed by the delamination process as shown in Fig. 1. The as-obtained $Ti_3C_2T_x$ aqueous suspension can be vacuum filtrated into freestanding films which can be directly used as electrodes for supercapacitors. During the filtration process, the $Ti_3C_2T_x$ nanoflakes restack layer by layer, which greatly hinders the electrolyte ion transport inside the film electrodes. Inspired by the laser reduction technique which is widely used for

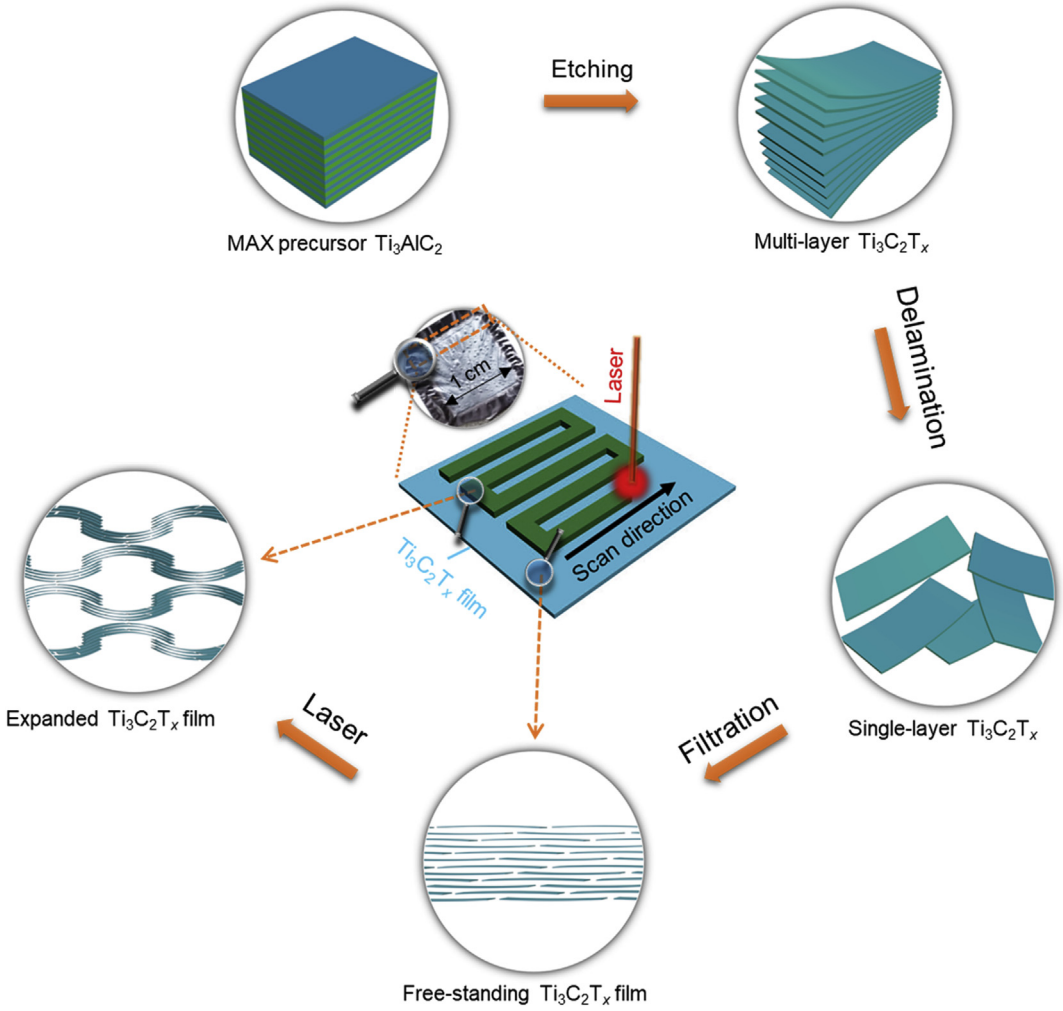


**Fig. 1.** Schematic illustration of the synthesis process. The flow shows the synthesis process of a laser written $Ti_3C_2T_x$ film starting from $Ti_3AlC_2$ precursor. The photographic image shows the color change of $Ti_3C_2T_x$ film before and after laser writing and the schematic in center shows the line-by-line laser scanning path. (For interpretation of the references to color in this figure legend, the reader is referred to the Web version of this article.)

reducing graphene oxides (GO) and alleviating the restacking of graphene-based electrodes, we successfully opened the restacked channels of $Ti_3C_2T_x$ nanosheets without damaging the integrity of the free-standing film by carefully tuning the laser output power density (by defocusing, as shown in Fig. S1, S2 and Table S1). Different from the reduction of GO after laser, the $Ti_3C_2T_x$ film can be oxidized with a color change from metallic purple to blue gray as shown in the photographic image of Fig. 1. The interlayer adsorbed $H_2O$ molecular are expected to be gasified by the fast photothermal process induced by laser and thus, opened structure of $Ti_3C_2T_x$ film is achieved. Actually, the bubbles evolved on the surface of laser written area is an evidence for the gasification (photographic image of Fig. 1). The schematic illustration shown in the center of Fig. 1 displays the line-by-line laser scanning path. Loose line gaps inevitably results in pristine $Ti_3C_2T_x$ as gaps left in the treated area. Therefore, in this section, the line gap is controlled to be 20 μm which is far smaller than the laser spot size so that all the $Ti_3C_2T_x$ can be covered.

By comparing the cross-sectional scanning electronic microscopy (SEM) images of $Ti_3C_2T_x$ free-standing films before and after laser writing, the restacked nanosheets are successfully opened up and the film thickness is increased to ~32 μm from ~2 μm (Fig. 2a and 2b). This mesoporous structure is alike to the expanded GO film after laser reduction [39].

Moreover, plenty of holes were created due to the photothermal oxidation of $Ti_3C_2T_x$ after laser writing (Fig. S3). The opened up porous structure induced by laser is expected to largely facilitate the ion transport inside the film and improve the rate performance thereby, as will be discussed below. The opening up of restacked $Ti_3C_2T_x$ nanosheets after laser writing can be possibly attributed to the gas evolution caused by the photothermal gasification of the interlayer trapped water molecular and part of surface groups. This may be also the reason for the "bubble" surface (photographic image of Fig. 1) and the decreased interlayer spacing (Fig. 2c) after laser writing. The new peaks after laser treatment shown in the X-ray diffraction (XRD) patterns are all shifted towards higher diffraction angles which means a decrease in the interlayer spacing. Such an opened-up structure and decreased interlayer spacing are schematically illustrated in Fig. 1. The centers of new peaks shown in Fig. 2c are increased almost linearly which satisfies the Bragg diffraction equation at small angles, indicating the 2D nature of the $Ti_3C_2T_x$ nanoflakes was well kept after laser writing. The $Ti_3C_2T_x$ was oxidized after laser which can be clearly observed from the Raman and X-ray photoelectronic spectroscopy (XPS) as shown in Fig. 2d and 2e. The peaks of the Raman spectra in the range of 200 $cm^{-1}$ to 800 $cm^{-1}$ can be assigned to the vibrations of $Ti_3C_2T_x$ and the peaks at 1350 $cm^{-1}$ and 1600 $cm^{-1}$ are related to the D and G band of carbon, respectively. The decrease of $Ti_3C_2T_x$ related peaks and the raise of carbon peaks after laser writing indicate that part of the $Ti_3C_2T_x$ were oxidized and converted into disordered carbon. $TiO_2$ is another oxidation product which is verified by the XPS results of Ti 2*p* orbit (centered at 459.0 eV) as shown in Fig. 2e. The peaks assigned to Ti in $Ti_3C_2T_x$ are still kept after laser, indicating that $Ti_3C_2T_x$ is only partially oxidized during the ultrafast photothermal process. To identify the changes of surface groups induced by laser, the XPS spectra of O 1s orbit are also analyzed as shown in Fig. 2f. The peaks at 529.8 eV, 531.1 eV, 532.2 eV and 533.3 eV can be assigned to the bonds of Ti–O, C–Ti-$O_x$, C–Ti-$OH_x$ and adsorbed $H_2O$, respectively [40]. It is obvious that the peaks of C–Ti-$OH_x$ and adsorbed $H_2O$ were relatively reduced after laser writing, an indicative of the removal of the –OH surface groups and adsorbed $H_2O$ molecular. In summary, the laser writing treatment of $Ti_3C_2T_x$ results in the formation of $TiO_2$ and carbons while maintaining the main conductive $Ti_3C_2T_x$ skeleton. Meanwhile, the –OH surface groups and adsorbed $H_2O$ molecular can be removed by laser, which resulted in the decrease in interlayer spacing and opening-up of the freestanding film due to the gas evolution during the writing process.

The cyclic voltammetry (CV) curves at 10 mV $s^{-1}$ show a pair of redox peaks which represents typical pseudocapacitive behavior of $Ti_3C_2T_x$ in $H_2SO_4$ aqueous electrolyte (Fig. 3a). The equation of this reversible redox reaction was reported to be as follows [41]:

$$Ti_3C_2O_x(OH)_yF_z + \delta e + \delta H^+ \rightleftharpoons Ti_3C_2O_{x-\delta}(OH)_{y+\delta}F_z$$

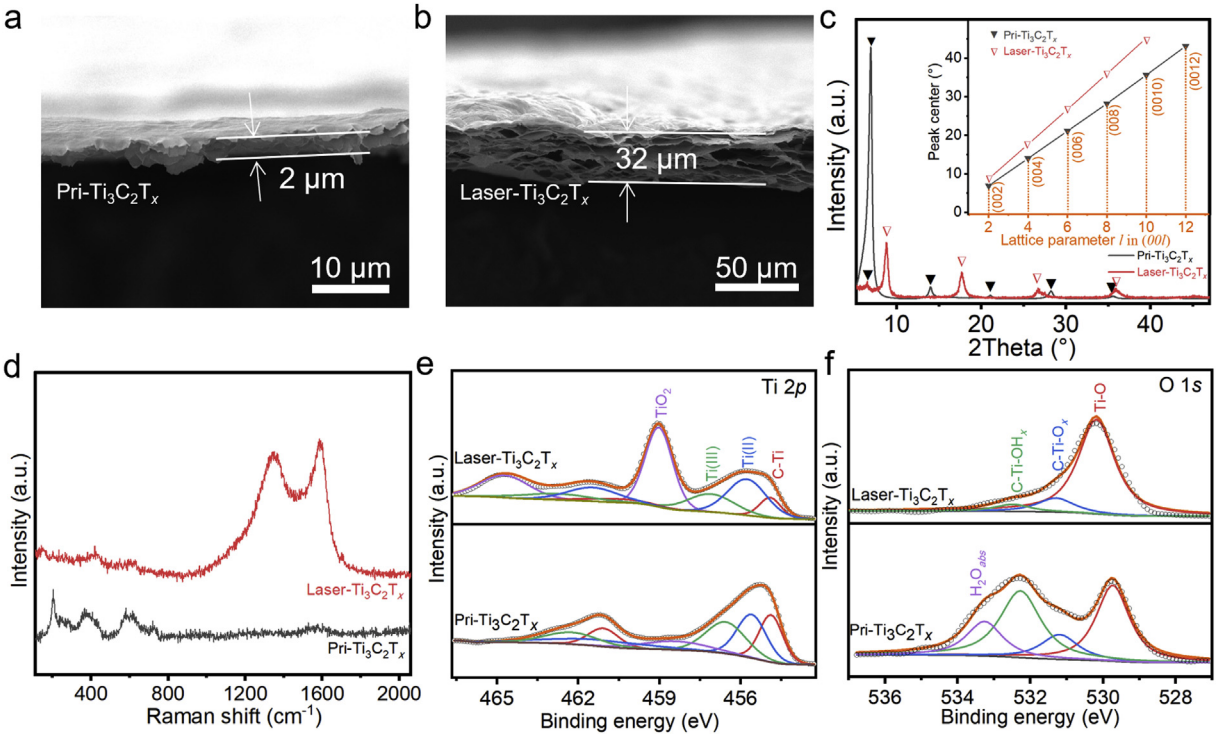


**Fig. 2.** Morphology and structure change induced by the laser writing. (a) cross-sectional SEM image of pristine $Ti_3C_2T_x$ (Pri-$Ti_3C_2T_x$) and (b) laser written $Ti_3C_2T_x$ (Laser-$Ti_3C_2T_x$). Comparison of (c) XRD patterns, (d) Raman spectra, (e) Ti 2*p* and (f) O1*s* XPS results before and after laser writing.

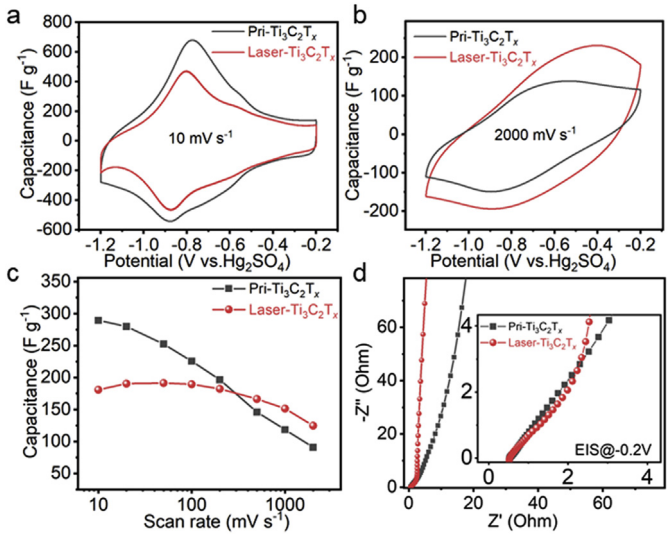


**Fig. 3.** Comparison of electrochemical performances before and after laser writing. comparison of CV curves (a) at 10 mV $s^{-1}$ and (b) 2000 mV $s^{-1}$, (c) rate performance and (d) EIS results.

The shape of the CV curve is not significantly changed after laser but with a decrease in the area of the curve, indicating a loss of specific capacitance. The capacitance loss can be ascribed to the partial oxidation of active $Ti_3C_2T_x$ into inactive $TiO_2$ and carbons. Nevertheless, the CV curve of laser written $Ti_3C_2T_x$ (Laser-$Ti_3C_2T_x$) at 2000 mV $s^{-1}$ shows a larger area than Pri-$Ti_3C_2T_x$, indicating higher capacitance of Laser-$Ti_3C_2T_x$ at high scan rates (Fig. 3b). The comparison of CV curves at different scan rates are displayed in Fig. S6. For better comparison, the discharge capacitances of $Ti_3C_2T_x$ before and after laser at different scan rates were calculated and displayed in Fig. 3c. The capacitance of $Ti_3C_2T_x$ at 10 mV $s^{-1}$ decreases rapidly to 182 F $g^{-1}$ after laser treatment from 290 F $g^{-1}$ in the Pri-$Ti_3C_2T_x$. However, the Laser-$Ti_3C_2T_x$ shows much improved rate performance with a capacitance retention of 69% at 2000 mV $s^{-1}$, the value of which is only 31% for Pri-$Ti_3C_2T_x$. Actually, Laser-$Ti_3C_2T_x$ shows an advantage in capacitance when the scan rate gets higher than 200 mV $s^{-1}$. The increase in rate performance can be ascribed to the porous and opened-up structure induced by laser where electrolyte ions are more accessible into the film electrode. From the electrochemical impedance spectra (EIS), it is obvious that the line at low frequencies turns more vertical (Fig. 3d) and the intercept on the *x*-axis keeps unchanged (inset of Fig. 3d), indicating again that the electrolyte ions became more accessible inside the $Ti_3C_2T_x$ film after laser without increasing the equivalent series resistance (ESR). The electronic conductivity of $Ti_3C_2T_x$ is still high after laser (~920 S $cm^{-1}$, Fig. S5) so that the rate performance will not be dominantly restricted by the electron transport process. As a result, the rate performance of $Ti_3C_2T_x$ can be effectively improved by the increased ion accessibility.

The laser writing process is further optimized in the pursuit of higher capacitance without compromising the rate performance, through controlling the laser line density, as shown in Fig. 4a. Since the gap between two adjacent laser scanning lines can be adjusted by software, it is convenient to adjust the effective area of laser scanning on $Ti_3C_2T_x$ film by controlling the line density (the line gap and line density are

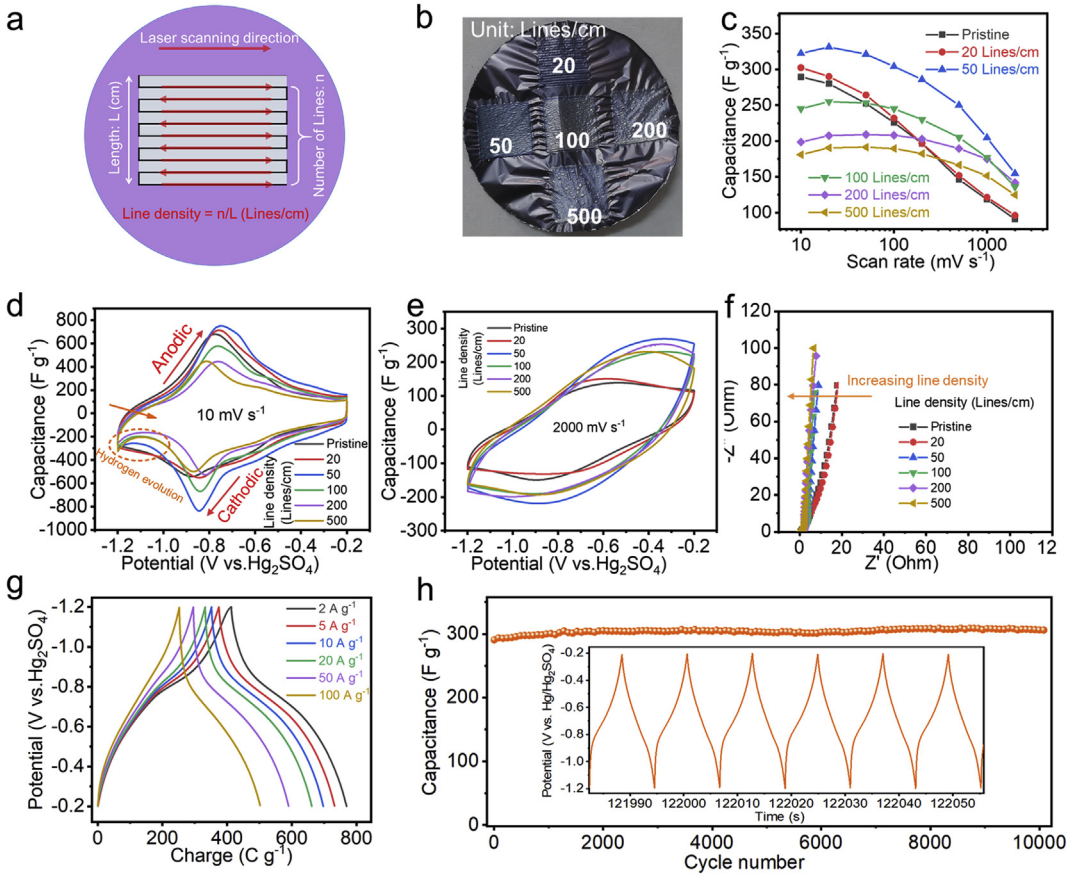


**Fig. 4.** Optimizing the electrochemical performance of laser written $Ti_3C_2T_x$. (a) Schematic showing the laser scanning path. (b) Photographic image of $Ti_3C_2T_x$ free-standing film written by laser written with different line densities. Comparison of (c) rate performance, (d) CV curves at 10 mV $s^{-1}$, (e) CV curves at 2000 mV $s^{-1}$ and (f) EIS of $Ti_3C_2T_x$ film electrode before and after laser writing with different line densities in the frequency range from $10^5$ to 0.1 Hz at a potential of −0.2 V vs. Hg/$Hg_2SO_4$. (g) Charge/discharge curves at different current densities and (h) cycling performance tested at 50 A $g^{-1}$ of Laser-$Ti_3C_2T_x$ with a line density of 50 Lines/cm.

reciprocal). Fig. 4b shows the photographic images of $Ti_3C_2T_x$ film treated by laser with different line densities. The line of laser scanning path can be clearly observed at a line density of 20 Lines/cm and more bubbles were formed on the surface with increase of line density (as shown in Fig. 4b), indicating more trapped water was gasified and more $Ti_3C_2T_x$ was oxidized. The line-line gaps determined by the SEM images are consistent with the line density as shown in Fig. S10. As a result, the electrochemical performance was successfully tuned by controlling the line density (Fig. 4c). The capacitance retention at 2000 mV $s^{-1}$ is 31%, 32%, 48%, 56%, 71% and 69% for $Ti_3C_2T_x$ films treated by laser with line density of 0 (pristine), 20, 50, 100, 200 and 500 Lines/cm, respectively. In general, the rate performance increases with line density, but the capacitance increases first and then decreases. It can be seen from Fig. 4c, when the line density increased to 50 Lines/cm, the capacitance at 10 mV $s^{-1}$ slightly increases and then drops rapidly when the line density further increased. As a result, the Laser-$Ti_3C_2T_x$ with a line density of 50 Lines/cm (~29 μm thick as shown in Fig. S11) shows highest capacitance at all scan rate range from 10 mV $s^{-1}$ to 2000 mV $s^{-1}$, even though the rate performance is not the best. However, the capacitance retention of laser-$Ti_3C_2T_x$ (50 Lines/cm) at 2000 mV $s^{-1}$ increased to 48% from 31% of the pristine one. By comparing with the anodic oxidized $Ti_3C_2T_x$ with an increased capacitance retention of 66% at 2000 mV $s^{-1}$ from 38%, it is reasonable to conclude that the rate performance improvement induced by the laser writing is comparable to the anodic oxidation, taking into account of the mass loading difference (~0.8 mg $cm^{-2}$ in this work and ~0.4 mg $cm^{-2}$ in the work of anodic oxidation) [32]. The $Ti_3C_2T_x$ films treated by laser with line density of 0 (pristine), 20, 50, 100, 200 and 500 Lines/cm show a capacitance of 289, 322, 302, 199, 181, 245 and 302 F $g^{-1}$ at 10 mV $s^{-1}$, respectively. The increase in capacitance at 10 mV $s^{-1}$ for Laser-$Ti_3C_2T_x$ with low line densities is a result of rate performance improvement instead of the intrinsic capacitance increase which has been discussed in our previous work [32].

It is very interesting that the capacitance of most laser treated $Ti_3C_2T_x$ at 20 mV $s^{-1}$ is slightly higher than that at 10 mV $s^{-1}$, which is abnormal. For the CV curves at cathodic process, we noticed that the current density abnormally increased from −1.1 V to −1.2 V for most of the laser written $Ti_3C_2T_x$ (Fig. 4d), which are generally ascribed to the hydrogen evolution. Part of $H^+$ ions that bonded to the $Ti_3C_2T_x$ surface in the pseudocapacitive reduction reaction may be consumed in the abnormal hydrogen evolution process and thus reduces the discharge capacitance at low scan rates. This may be the reason for the abnormal increase of capacitance from 10 mV $s^{-1}$ to 20 mV $s^{-1}$, but the insight mechanism needs to be further discovered. The CV curves at 2000 mV $s^{-1}$ are shown in Fig. 4e. The increased area of the curves after laser writing indicates higher capacitance, which is consistence with the results in the rate performance (Fig. 4c). The diffusion-controlled and capacitive contributions to the total charge storage were calculated and displayed in Fig. S8 by using the CV results of Pri-$Ti_3C_2T_x$ and Laser-$Ti_3C_2T_x$ (50 Lines/cm) at the scan rates from 10 to 100 mV $s^{-1}$ (Fig. S7). The methods for the calculations are presented in the Experiment details in the Supporting Information. It is obvious that the capacitive contributions are significantly increased after laser writing at various scan rates, showing high consistence with the results of rate performance evaluations. The slope of the line at low frequencies of the EIS results increases with the increase of the laser scanning line density (Fig. 4f), indicating higher ion accessibility and better rate capability. The calculated time constants (based on the EIS data) of $Ti_3C_2T_x$ films treated by laser with line density of 0 (pristine), 20, 50, 100, 200 and 500 Lines/cm are 3.23, 3.23, 0.38, 0.31, 0.21 and 0.24 s, respectively (Fig. S9). Since the Laser-$Ti_3C_2T_x$ with a line density of 50 Lines/cm shows the best optimized electrochemical performance, the galvanostatic charge and discharge (GCD) rate performance and cycle life were further tested with this sample. The charge/discharge curves are displayed in Fig. 4g. The capacitance retention at 100 A $g^{-1}$ is as high as 70% by comparing the value at 2 A $g^{-1}$, indicating high rate performance, which is consistent with the CV results. This film electrode also showed excellent cyclic stability which showed a 105% capacitance retention after 10000 cycles (Fig. 4h). The slightly increase in capacitance after cycles may be a result of room temperature change. The charge/discharge curve after cycles keeps almost intact, showing great cycle performance.

To evaluate the practical performance of Laser-$Ti_3C_2T_x$ (50 Lines/cm), the electrochemical performance of $Ti_3C_2T_x$-based symmetric micro-supercapacitors (MSC) are further compared as shown in Fig. 5. The process for MSC fabrication is given in the experimental details in the Supporting Information. The Laser-$Ti_3C_2T_x$-based MSCs with interdigital fingers vertical or parallel to the laser scanning direction are abbreviated as Laser-$Ti_3C_2T_x$(⊥) and Laser-$Ti_3C_2T_x$(||), respectively. The photographic images and schematic illustrations of $Ti_3C_2T_x$-based MSCs are shown in

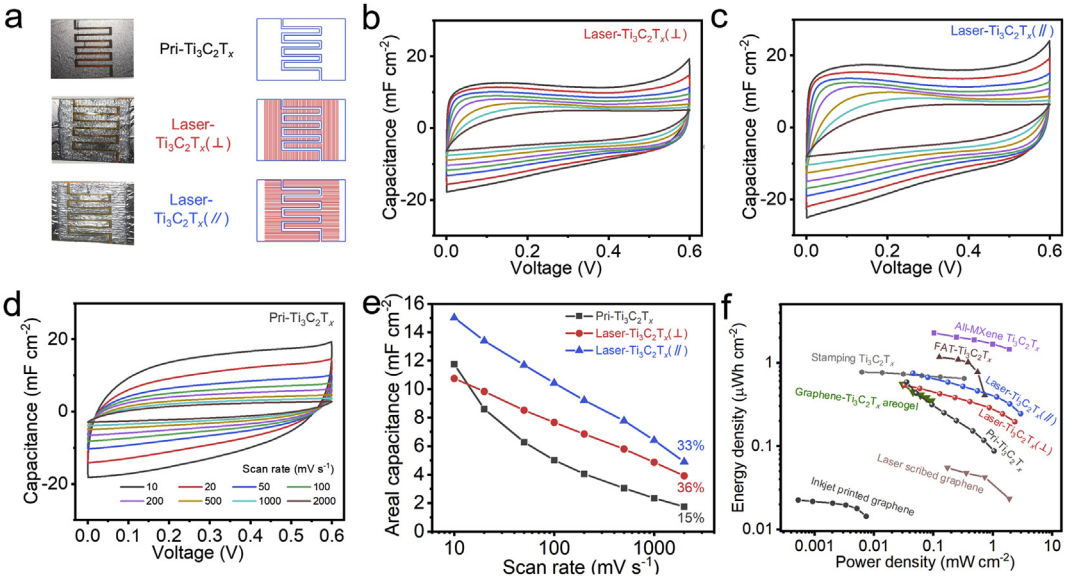


**Fig. 5.** Electrochemical performance of $Ti_3C_2T_x$-based symmetric micro-supercapacitors. (a) Photographic images and schematic illustrations of the difference between pristine and laser treated $Ti_3C_2T_x$ micro-supercapacitors. The $Ti_3C_2T_x$ micro-supercapacitors with interdigital fingers vertical and parallel to the laser scanning direction are named as Laser-$Ti_3C_2T_x$(⊥) and Laser-$Ti_3C_2T_x$(||), respectively. (b) CV curves of Pri-$Ti_3C_2T_x$, (c) Laser-$Ti_3C_2T_x$(⊥) and (d) Laser-$Ti_3C_2T_x$(||). (e) comparison of rate performance and (f) areal energy density vs. areal power density for different micro-supercapacitors.

Fig. 5a. The shadow area with red lines (laser scanning lines) refers to the laser written area. CV curves were tested at different scan rates within a voltage window of 0.6 V in 3 M $H_2SO_4$ electrolyte (Fig. 5b–d). The voltage window of the symmetric MSC devices is only 0.6 V which is mainly limited by the upper potential limit of the $Ti_3C_2T_x$ in $H_2SO_4$ electrolyte. When the voltage goes higher than 0.6V, the oxidation of the $Ti_3C_2T_x$ takes place before the electrolyte decomposition. All the CV curves at low scan rates show a rectangular-like shape, indicating EDL capacitive behavior in this voltage window. The MSCs with laser written $Ti_3C_2T_x$ electrodes shows larger area in CV curves at 2000 mV $s^{-1}$, exhibiting rate capability advantages over pristine one. For better comparison, the rate performance of different MSCs are compared in Fig. 5e. The pri-$Ti_3C_2T_x$ MSC shows an areal capacitance of 11.75 mF $cm^{-2}$ at 10 mV $s^{-1}$ and a capacitance retention of only 15% at 2000 mV $s^{-1}$. The Laser-$Ti_3C_2T_x$(⊥) shows relative lower capacitance (11.75 mF $cm^{-2}$) at 10.

mV $s^{-1}$ but a highest capacitance retention of 36% at 2000 mV $s^{-1}$, which can be ascribed to the more optimal structure for electrolyte ion penetration. The Laser-$Ti_3C_2T_x$(||) shows a highest areal capacitance of 15.03 mF $cm^{-2}$ at 10 mV $s^{-1}$ with comparable retention of 33% at 2000 mV $s^{-1}$. The high areal capacitances at such high scan rates enables $Ti_3C_2T_x$-based MSCs to deliver high areal energy densities at high power densities (Fig. 5f). The energy density of Laser-$Ti_3C_2T_x$(||) is as high as 0.25 μWh $cm^{-2}$ at an ultrahigh power density of 2.94 mW $cm^{-2}$, while the Pri-$Ti_3C_2T_x$ MSC can deliver only 0.09 μWh $cm^{-2}$ at 1.05 mW $cm^{-2}$. Both the areal energy density and areal power density of $Ti_3C_2T_x$-based MSCs in this work are much higher than the performance of inkjet-printed graphene [42]. For a typical laser reduced graphene MSC in aqueous electrolyte, the energy density is only 0.02 μWh $cm^{-2}$ at similar high power density of 1.89 mW $cm^{-2}$ [39]. By comparing with other symmetric MSCs with additive-free $Ti_3C_2T_x$-based electrodes (without any current collectors), the energy density and power density obtained in our work are very close to the values of the reported ones ($Ti_3C_2T_x$-graphene aerogel [43], stamping $Ti_3C_2T_x$ [44], FAT-$Ti_3C_2T_x$ [45] and All-MXene $Ti_3C_2T_x$ [46]). It is expected that the laser writing technique may be applicable to the $Ti_3C_2T_x$-based MSCs with other configurations as well and further improves the already reported performance.

## 3. Conclusions

The laser writing technique was successfully applied to alleviate the restacking of $Ti_3C_2T_x$ by opening up the channels of restacked nanosheets and creating holes. As a result, the rate performance of $Ti_3C_2T_x$ was effectively improved. By tuning the line density of laser scanning path, the best optimized electrochemical performance was obtained, showing both high capacitance and high rate capability. The laser writing is an ultrafast, contactless and chemical free technique for alleviating the restacking of $Ti_3C_2T_x$, showing incomparable advantage among all the reported methods. This work highlights the importance of restructured ion channels and indicates a great promise of laser writing strategy in achieving high-performance supercapacitors at much reduced time and cost.

## CRediT authorship contribution statement

**Jun Tang:** Conceptualization, Methodology, Data curation, Software, Formal analysis, Writing - original draft, Writing - review & editing. **Wendi Yi:** Methodology, Data curation. **Xiongwei Zhong:** Methodology, Data curation. **Chuanfang (John) Zhang:** Methodology, Writing - review & editing. **Xu Xiao:** Methodology, Writing - review & editing. **Feng Pan:** Supervision, Methodology, Writing - review & editing. **Baomin Xu:** Supervision, Methodology, Funding acquisition.

## Declaration of competing interest

The authors declare that they have no known competing financial interests or personal relationships that could have appeared to influence the work reported in this paper.

## Acknowledgments

This work was financially supported by the Fundamental Research (Discipline Arrangement) project funding from Shenzhen Science and Technology Innovation Committee (Grant No. JCYJ20170412154554048), the Peacock Team Project from Shenzhen Science and Technology Innovation Committee (Grant No. KQTD2015033110182370), and the National Key Research and Development Project from the Ministry of Science and Technology of China (Grants Nos. 2016YFA0202400 and 2016YFA0202404).

## Appendix A. Supplementary data

Supplementary data to this article can be found online at https://doi.org/10.1016/j.ensm.2020.07.028.

## References

[1] P. Simon, Y. Gogotsi, Materials for electrochemical capacitors, Nat. Mater. 7 (2008) 845–854.
[2] T. Liu, Y. Li, Addressing the Achilles' heel of pseudocapacitive materials: long-term stability, InfoMat (2020) 1–36, n/a.
[3] K. Li, X. Wang, S. Li, P. Urbankowski, J. Li, Y. Xu, Y. Gogotsi, An ultrafast conducting Polymer@MXene positive electrode with high volumetric capacitance for advanced asymmetric supercapacitors, Small 16 (2020) 1906851.
[4] B. Liu, S. Sun, R. Jia, H. Zhang, X. Zhu, C. Zhang, J. Xu, T. Zhai, H. Xia, Oxygen-deficient homo-interface toward exciting boost of pseudocapacitance, Adv. Funct. Mater. 30 (2020) 1909546.
[5] Z. Li, S. Gadipelli, H. Li, C.A. Howard, D.J.L. Brett, P.R. Shearing, Z. Guo, I.P. Parkin, F. Li, Tuning the interlayer spacing of graphene laminate films for efficient pore utilization towards compact capacitive energy storage, Nature Energy 5 (2020) 160–168.
[6] Murat Ates, Ozge Kuzgun, Murat yıldırım, Ozan Yoruk, Yuksel Bayrak, Supercapacitor performances of RuO2/MWCNT, RuO2/Fullerene nanocomposites, Energy Storage 1 (2019) e86, 1.
[7] J. Zhao, F. Liu, W. Li, Phosphate ion-modified RuO2/Ti3C2 composite as a high-performance supercapacitor, Material, Nanomaterials 9 (2019) 377.
[8] Q. Zhang, D. Zhang, Z. Miao, X. Zhang, S. Chou, Research progress in MnO2 -carbon based supercapacitor electrode materials, Small 24 (2018) 1702883.
[9] A. Heather, Andreas, bringing real-world energy-storage Research into a second-year physical-chemistry lab using a MnO2-based supercapacitor, J. Chem. Educ. 95 (2018) 2028–2033, págs.
[10] Y. Ge, Exploring electrolyte preference of vanadium nitride supercapacitor electrodes, Mater. Res. Bull. 76 (2016) 37–40.
[11] H. Liu, H. Zhang, H. Xu, T. Lou, Z. Sui, Y. Zhang, In situ self-sacrificed template synthesis of vanadium nitride/nitrogen-doped graphene nanocomposites for electrochemical capacitors, Nanoscale 10 (2018) 5246.
[12] C. Zhao, X. Jia, K. Shu, C. Yu, G.G. Wallace, C. Wang, Conducting polymer composites for unconventional solid-state supercapacitors, J. Mater. Chem. A. 8 (2020) 4677–4699.
[13] Z. Li, L. Gong, Research progress on applications of polyaniline (PANI) for electrochemical energy storage and conversion, Materials 13 (2020) 548.
[14] A. Ponrouch, S. Garbarino, E. Bertin, D. Guay, Ultra high capacitance values of Pt@RuO2 core–shell nanotubular electrodes for microsupercapacitor applications, J. Power Sources 221 (2013) 228–231.
[15] S. Zhai, C. Wang, H.E. Karahan, Y. Wang, X. Chen, X. Sui, Q. Huang, X. Liao, X. Wang, Y. Chen, Nano-RuO2-Decorated holey graphene composite fibers for micro-supercapacitors with ultrahigh energy density, Small 14 (2018) 1800582.
[16] K.P. Annamalai, X. Zheng, J. Gao, T. Chen, Y. Tao, Nanoporous ruthenium and manganese oxide nanoparticles/reduced graphene oxide for high-energy symmetric supercapacitors, Carbon 144 (2019) 185–192.
[17] D. Gueon, J.H. Moon, MnO2 nanoflake-shelled carbon nanotube particles for high-performance supercapacitors, ACS Sustain. Chem. Eng. 5 (2017) 2445–2453.
[18] B. Anasori, Y. Gogotsi (Eds.), 2D Metal Carbides and Nitrides (MXenes): Structure, Properties and Applications, Springer International Publishing, 2019. June 18, 2019, https://www.springer.com/gp/book/9783030190255.
[19] G. Gao, A.P. O'Mullane, A. Du, 2D MXenes: a new family of promising catalysts for the hydrogen evolution reaction, ACS Catal. 7 (2017) 494–500.
[20] M. Ghidiu, M.R. Lukatskaya, M.-Q. Zhao, Y. Gogotsi, M.W. Barsoum, Conductive two-dimensional titanium carbide 'clay' with high volumetric capacitance, Nature 516 (2014) 78–81.
[21] F. Shahzad, M. Alhabeb, C.B. Hatter, B. Anasori, S.M. Hong, C.M. Koo, Y. Gogotsi, Electromagnetic interference shielding with 2D transition metal carbides (MXenes), Science 353 (2016) 1137–1140.
[22] D. Er, J. Li, M. Naguib, Y. Gogotsi, V.B. Shenoy, Ti3C2 MXene as a high capacity electrode material for metal (Li, Na, K, Ca) ion batteries, ACS Appl. Mater. Interfaces 6 (2014) 11173–11179.

[23] X. Xiao, P. Urbankowski, K. Hantanasirisakul, Y. Yang, S. Sasaki, L. Yang, C. Chen, H. Wang, L. Miao, S.H. Tolbert, S.J.L. Billinge, H.D. Abruña, S.J. May, Y. Gogotsi, Scalable synthesis of ultrathin Mn3N2 exhibiting room-temperature antiferromagnetism, Adv. Funct. Mater. 29 (2019) 1809001.
[24] X. Xiao, H. Wang, P. Urbankowski, Y. Gogotsi, Topochemical synthesis of 2D materials, Chem. Soc. Rev. 47 (2018) 8744–8765.
[25] X. Xiao, H. Wang, W. Bao, P. Urbankowski, L. Yang, Y. Yang, K. Maleski, L. Cui, S.J.L. Billinge, G. Wang, Y. Gogotsi, Two-dimensional arrays of transition metal nitride nanocrystals, Adv. Mater. 31 (2019) 1902393.
[26] X. Zhang, J. Miao, P. Zhang, Q. Zhu, M. Jiang, B. Xu, 3D crumbled MXene for high-performance supercapacitors, Chin. Chem. Lett. (2020), https://doi.org/10.1016/j.cclet.2020.03.040. In press.
[27] Y. Zhu, K. Rajouâ, S. Le Vot, O. Fontaine, P. Simon, F. Favier, Modifications of MXene layers for supercapacitors, Nano Energy 73 (2020) 104734.
[28] M.R. Lukatskaya, O. Mashtalir, C.E. Ren, Y. Dall'Agnese, P. Rozier, P.L. Taberna, M. Naguib, P. Simon, M.W. Barsoum, Y. Gogotsi, Cation intercalation and high volumetric capacitance of two-dimensional titanium carbide, Science 341 (2013) 1502–1505.
[29] M. Naguib, M. Kurtoglu, V. Presser, J. Lu, J. Niu, M. Heon, L. Hultman, Y. Gogotsi, M.W. Barsoum, Two-dimensional nanocrystals produced by exfoliation of Ti3AlC2, Adv. Mater. 23 (2011) 4248–4253.
[30] J. Zhang, N. Kong, S. Uzun, A. Levitt, S. Seyedin, P.A. Lynch, S. Qin, M. Han, W. Yang, J. Liu, X. Wang, Y. Gogotsi, J.M. Razal, Scalable manufacturing of free-standing, strong Ti3C2Tx MXene films with outstanding conductivity, Adv. Mater. (2020) 2001093, n/a.
[31] M.R. Lukatskaya, S. Kota, Z. Lin, M.-Q. Zhao, N. Shpigel, M.D. Levi, J. Halim, P.-L. Taberna, M.W. Barsoum, P. Simon, Y. Gogotsi, Ultra-high-rate pseudocapacitive energy storage in two-dimensional transition metal carbides, Nature Energy 2 (2017) 17105.
[32] J. Tang, T.S. Mathis, N. Kurra, A. Sarycheva, X. Xiao, M.N. Hedhili, Q. Jiang, H.N. Alshareef, B. Xu, F. Pan, Y. Gogotsi, Tuning the electrochemical performance of titanium carbide MXene by controllable in situ anodic oxidation, Angew. Chem. Int. Ed. 58 (2019) 17849–17855.
[33] S.B. Ambade, R.B. Ambade, W. Eom, S.H. Noh, S.H. Kim, T.H. Han, 2D Ti3C2 MXene/WO3 hybrid architectures for high-rate supercapacitors, Advanced Materials Interfaces 5 (2018) 1801361.
[34] X. Zhang, R. Lv, A. Wang, W. Guo, X. Liu, J. Luo, MXene aerogel scaffolds for high-rate lithium metal anodes, Angew. Chem. 130 (2018) 15248–15253.
[35] J. Yan, C.E. Ren, K. Maleski, C.B. Hatter, B. Anasori, P. Urbankowski, A. Sarycheva, Y. Gogotsi, Flexible MXene/graphene films for ultrafast supercapacitors with outstanding volumetric capacitance, Adv. Funct. Mater. 27 (2017) 1701264.
[36] M.-Q. Zhao, C.E. Ren, Z. Ling, M.R. Lukatskaya, C. Zhang, K.L.V. Aken, M.W. Barsoum, Y. Gogotsi, Flexible MXene/carbon nanotube composite paper with high volumetric capacitance, Adv. Mater. 27 (2015) 339–345.
[37] E. Kayali, A. VahidMohammadi, J. Orangi, M. Beidaghi, Controlling the dimensions of 2D MXenes for ultrahigh-rate pseudocapacitive energy storage, ACS Appl. Mater. Interfaces 10 (2018) 25949–25954.
[38] C.E. Ren, M.-Q. Zhao, T. Makaryan, J. Halim, M. Boota, S. Kota, B. Anasori, M.W. Barsoum, Y. Gogotsi, Porous two-dimensional transition metal carbide (MXene) flakes for high-performance Li-ion storage, ChemElectroChem 3 (2016) 689–693.
[39] M.F. El-Kady, V. Strong, S. Dubin, R.B. Kaner, Laser scribing of high-performance and flexible graphene-based electrochemical capacitors, Science 335 (2012) 1326–1330.
[40] A. Agresti, A. Pazniak, S. Pescetelli, A. Di Vito, D. Rossi, A. Pecchia, M. Auf der Maur, A. Liedl, R. Larciprete, D.V. Kuznetsov, D. Saranin, A. Di Carlo, Titanium-carbide MXenes for work function and interface engineering in perovskite solar cells, Nat. Mater. 18 (2019) 1228–1234.
[41] M.R. Lukatskaya, S.-M. Bak, X. Yu, X.-Q. Yang, M.W. Barsoum, Y. Gogotsi, Probing the mechanism of high capacitance in 2D titanium carbide using in situ X-ray absorption spectroscopy, Advanced Energy Materials 5 (2015) 1500589.
[42] S.S. Delekta, K.H. Adolfsson, N.B. Erdal, M. Hakkarainen, M. Östling, J. Li, Fully inkjet printed ultrathin microsupercapacitors based on graphene electrodes and a nano-graphene oxide electrolyte, Nanoscale 11 (2019) 10172–10177.
[43] Y. Yue, N. Liu, Y. Ma, S. Wang, W. Liu, C. Luo, H. Zhang, F. Cheng, J. Rao, X. Hu, J. Su, Y. Gao, Highly self-healable 3D microsupercapacitor with MXene–graphene composite aerogel, ACS Nano 12 (2018) 4224–4232.
[44] C.( John, Zhang, M.P. Kremer, A. Seral-Ascaso, S.-H. Park, N. McEvoy, B. Anasori, Y. Gogotsi, V. Nicolosi, Stamping of flexible, coplanar micro-supercapacitors using MXene inks, Adv. Funct. Mater. 28 (2018) 1705506.
[45] X. Huang, P. Wu, A Facile, High-Yield, and Freeze-and-Thaw-Assisted Approach to Fabricate MXene with Plentiful Wrinkles and Its Application in On-Chip Micro-Supercapacitors, Adv. Funct. Mater. 30 (2020) 1910048.
[46] Y.-Y. Peng, B. Akuzum, N. Kurra, M.-Q. Zhao, M. Alhabeb, B. Anasori, E.C. Kumbur, H.N. Alshareef, M.-D. Ger, Y. Gogotsi, All-MXene (2D titanium carbide) solid-state microsupercapacitors for on-chip energy storage, Energy Environ. Sci. 9 (2016) 2847–2854.